Journal of Materials Chemistry A

Incorporation of Alkylthio Side Chains on Benzothiadiazole-based Non-fullerene Acceptors Enables High-performance Organic Solar Cells with over 16% Efficiency

Journal:	*Journal of Materials Chemistry A*
Manuscript ID	TA-COM-09-2020-008830.R1
Article Type:	Communication
Date Submitted by the Author:	12-Oct-2020
Complete List of Authors:	Cheung, Andy Man Hong; Hong Kong University of Science and Technology, Chemistry Yu, Han; The Hong Kong University of Science and Technology, Chemistry Luo, Siwei; Hong Kong University of Science and Technology Wang, Zhen; North Carolina State University, Physics Qi, Zhenyu; Hong Kong University of Science and Technology, Chemistry Zhou, Wentao; Hong Kong University of Science and Technology Arunagiri, Lingeswaran; HKUST Chang, Yuan; Hong Kong University of Science and Technology, Chemistry Yao, Huatong; The Hong Kong University of Science and Technology, Department of Chemistry Ade, Harald; North Carolina State University, Department of Physics Yan, He; The Hong Kong University of Science and Technology, Department of Chemistry

Incorporation of Alkylthio Side Chains on Benzothiadiazole-based Non-fullerene Acceptors Enables High-performance Organic Solar Cells with over 16% Efficiency

Andy Man Hong Cheung [§, ⊥], Han Yu [§, ⊥, *], Siwei Luo [§, ⊥], Zhen Wang [#], Zhenyu Qi [§], Wentao Zhou [§], Lingeswaran Arunagiri [§], Yuan Chang [§], Huatong Yao [§,*], Harald Ade [#,*], He Yan [§, ‡, $, *]

[§] Department of Chemistry and Hong Kong Branch of Chinese National Engineering Research Center for Tissue Restoration and Reconstruction, Hong Kong University of Science and Technology, Clear Water Bay, Kowloon, Hong Kong

[#] Department of Physics and Organic and Carbon Electronics Laboratories (ORaCEL), North Carolina State University, Raleigh, NC 27695, USA

[‡] Hong Kong University of Science and Technology-Shenzhen Research Institute, No. 9, Yuexing 1st RD, Hi-tech Park, Nanshan, Shenzhen 518057, China

[$] Institute of Polymer Optoelectronic Materials and Devices, State Key Laboratory of Luminescent Materials and Devices, South China University of Technology, Guangzhou 510640, China

[⊥]These authors contributed equally to this work.

ABSTRACT

Y6-type non-fullerene acceptors (NFAs) with an acceptor-donor-acceptor'-donor-acceptor (A-D-A'-D-A) structure have been very popular in the field of organic solar cells (OSCs) due to their excellent performances. In this study, two novel NFAs, BTPS-4F and BTPS-4Cl were designed by incorporating undecylthio side chains into a thienothiophene moiety and connecting it to two different halogenated 2-(3-oxo-2,3-dihydroinden-1-ylidene)malononitrile end groups (2F-IC and 2Cl-IC) respectively. When blended with a donor polymer, PM6, BTPS-4F-based devices achieved a high power conversion efficiency (PCE) up to 16.2% with an open-circuit voltage (V_{OC}) of 0.82 V, a short-circuit current density (J_{SC}) of 25.2 mA cm^{-2} and a fill factor (FF) of 0.78, while BTPS-4Cl-based devices achieved an inferior PCE of 13.5%. This is the first time alkylthio chains are employed on Y6-like NFAs to achieve high-performance OSCs. Subsequent characterizations showed that the upshifted energy level of BTPS-4F and the better intermolecular packing in PM6:BTPS-4F blends are the major reasons for the enhanced performance of BTPS-4F-based devices over BTPS-4Cl-based ones. This work provides high-performance non-fullerene acceptors for OSCs and demonstrates a promising molecular design strategy that can effectively regulate the energy levels and morphology.

INTRODUCTION

Extensive research effort from both academia and industry has been devoted to the development of OSCs due to their unique advantages, such as light weight, transparency, mechanical flexibility and roll-to-roll production feasibility.[1–3] Compared to conventional fullerene derivative acceptors, non-fullerene acceptors (NFAs) have been proved to demonstrate excellent absorption, improved chemical tunability, reduced voltage loss (V_{loss}), low cost and decent stability in bulk heterojunction (BHJ) blends.[4–7] Recently, multiple research groups have reported PCEs over 17% achieved by NFA-based OSCs, proving the huge application potential of OSCs in the future.[8–16]

A popular and promising approach is to adopt an acceptor-donor-acceptor'-donor-acceptor (A-D-A'-D-A) structure with tunable side chains and end groups to achieve small molecule acceptors (SMAs) with desirable energy levels, absorption and morphology.[17–19] This approach led to an outstanding material Y6 which could achieve a V_{OC} of 0.83 V, a J_{sc} of 25.3 mA cm^{-2}, a FF of 74.8% and a PCE of 15.7%.[20] Since then, numerous attempts have been made to optimize Y6 and devices based on it.[21–26]

Recent studies have suggested that alkylthio side chain is a desirable structural motif because the upshifted LUMO (due to the introduction of electron-donating sulfur atoms) decreases energy loss incurred during exciton dissociation.[27,28] The lone pairs on sulfur also increase the electron-donating ability of the donor motifs (such as thiophene and thieno[3,2-b]thiophene (TT)), resulting in an enhanced intramolecular charge transfer (ICT) effect.[29–32] When blended with an appropriate donor, these phenomena can improve the external quantum efficiency (EQE), J_{SC}, and ultimately device performance. On the other hand, computational and experimental studies have also shown that sulfur atoms exhibit S-S and S-π interactions.[33–36] Since sulfur atoms are commonly found in many optoelectronic materials and side-chain engineering is a common approach to improve intermolecular packing, it is anticipated that alkylthio chains on NFAs can facilitate BHJ formation while maintaining a good domain purity, leading to a high FF and PCE.[37–40]

With these considerations, we examined the effect of alkylthio chains on Y-series NFAs for the first time. Two novel Y-series acceptors with undecylthio side chains at a TT moiety and end-capped with different halogenated end groups (2F-IC and 2Cl-IC), namely BTPS-4F and BTPS-4Cl, were designed and systematically investigated (**Figure 1**). OSC devices were fabricated using

a conventional structure by blending the donor polymer PM6 with the respective SMAs. Devices based on BTPS-4F achieved a V_{OC} of 0.82 V, a J_{SC} of 25.2 mA cm^{-2}, a FF of 0.78 and a PCE of 16.2%, whereas devices based on BTPS-4Cl achieved a V_{OC} of 0.81 V, a J_{SC} of 24.3 mA cm^{-2}, a FF of 0.69 and a PCE of 13.5%. BTPS-4F-based devices demonstrated a better PCE and comparable performance parameters than Y6-based ones when they were first reported. The upshifted lowest unoccupied molecular orbital (LUMO) level of BTPS-4F and the enhanced intermolecular packing in PM6:BTPS-4F blends were found to be the major reasons for the superior performance of BTPS-4F-based devices over that of BTPS-4Cl-based devices. Our work has shed light on the structure-performance relationship of alkylthio chain-substituted Y6-type SMAs and suggested the potential application of such strategy in designing active layer materials for OSCs.

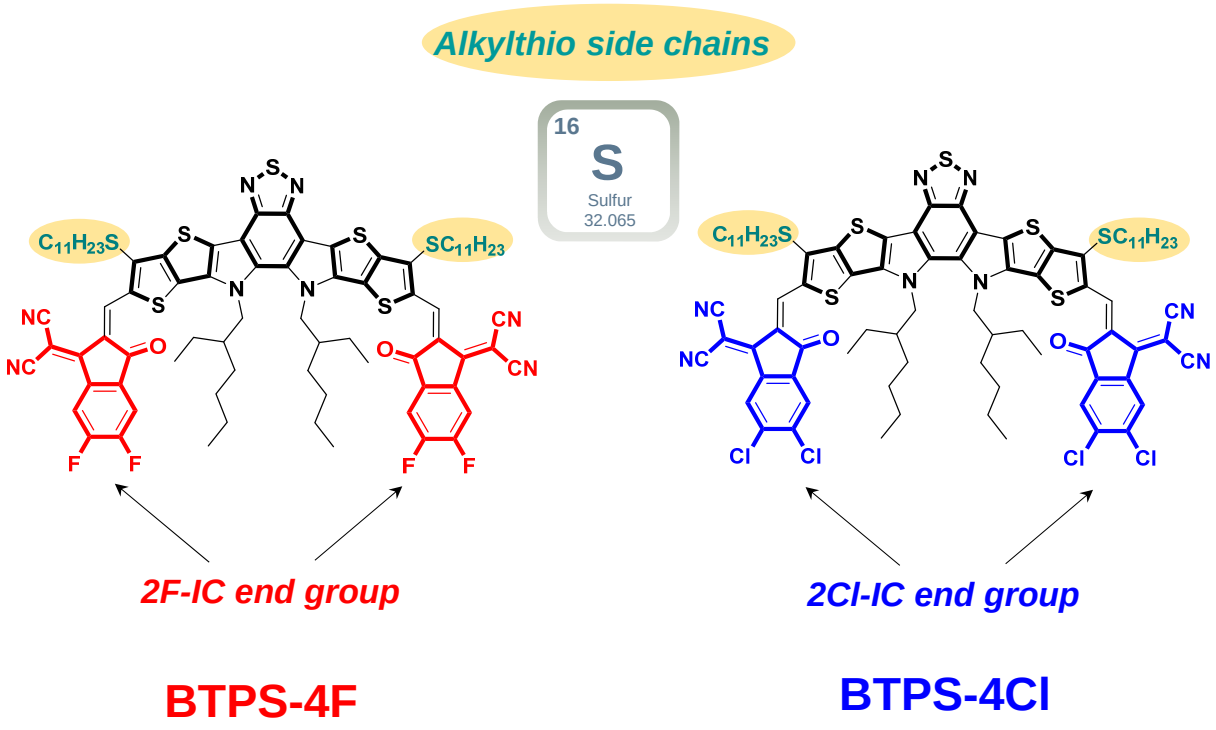

Figure 1. Chemical structures of BTPS-4F and BTPS-4Cl.

RESULTS AND DISCUSSIONS

Scheme 1 depicts the synthetic routes to BTPS-4F and BTPS-4Cl. Sulfur atoms were introduced in the first step, during which 3-bromothieno[3,2-b]thiophene was activated by *n*-butyl lithium (*n*-BuLi) and sulfur powder (S_8) was used as the sulfur source. Subsequent addition of 1-bromoundecane then completed the addition of alkylthio chain. The alkylthio chain was found to be air-stable and unaffected by heat or other reagents in subsequent synthetic steps, suggesting incorporation of alkylthio chains is a feasible approach to design and synthesize other SMAs. Then, other steps were conducted according to previously reported literature.[20] 2F-IC or 2Cl-IC end groups were used to yield BTPS-4F and BTPS-4Cl.[41,42] All target compounds were characterized by ^{1}H NMR, ^{13}C NMR and mass spectroscopy, which are summarized in the Supporting Information. The thermal decomposition temperatures (T_d) derived from thermogravimetric analysis (TGA, at 5% weight loss, **Figure S1**) (BTPS-4F: 315 °C, BTPS-4Cl: 299 °C) indicates that both molecules are stable under high temperature and thus suitable for OSC operation.

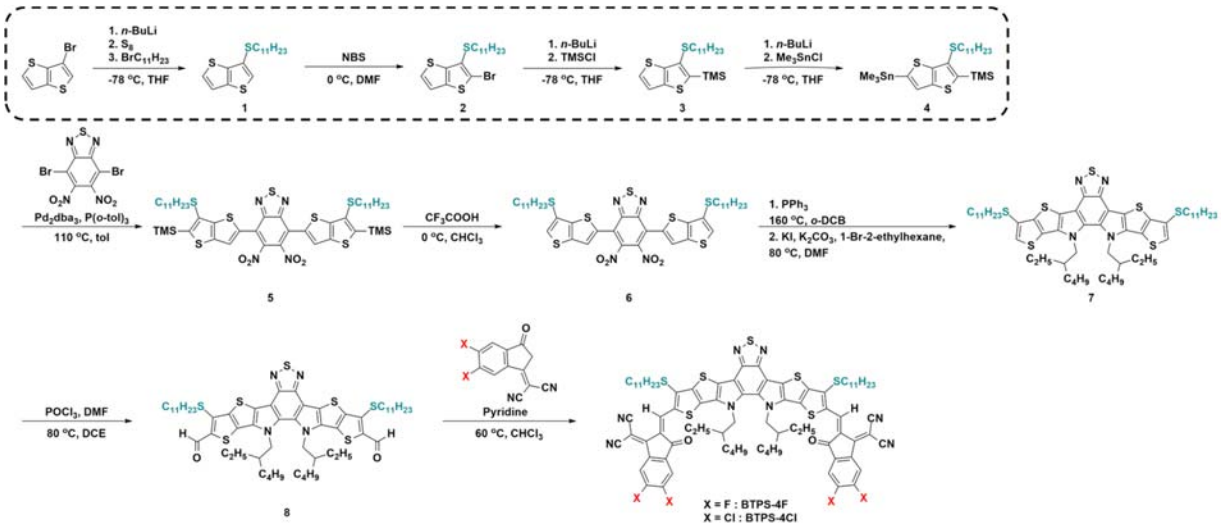

Scheme 1. Synthetic routes to BTPS-4F (X = F) and BTPS-4Cl (X = Cl)

To elucidate the effects of alkylthio chains, density functional theory (DFT) calculations were employed at B3LYP/6-31G (d,p) level to study the geometries and frontier molecular orbitals (FMOs) of the SMAs. To simplify the calculations, the undecylthio and 2-ethylhexyl chains were replaced by methylthio and 2-methylpropyl groups respectively. **Figure 2** shows that BTPS-4F has a larger bandgap and upshifted energy levels compared to BTPS-4Cl. Also, both BTPS-4F and BTPS-4Cl have a helical backbone with a small dihedral angle (BTPS-4F: 14.8°, BTPS-4Cl: 15.0°)

between the two flanks of the molecules. These are desirable factors that imply BTPS-4F and BTPS-4Cl can exhibit optimal intermolecular packing. Moreover, the FMOs spread across the entire molecule, implying good conjugation across the entire π framework, facilitating charge transport within and across molecules.

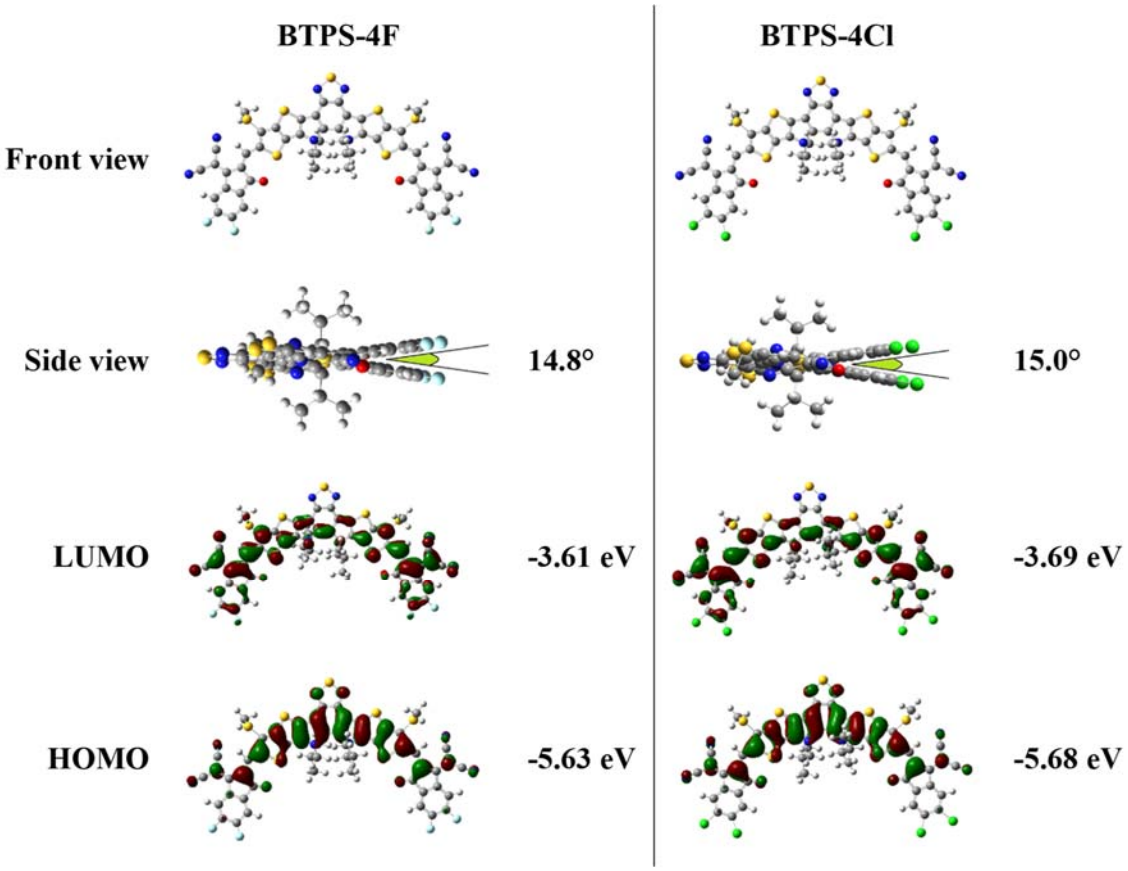

Figure 2. Optimized geometries and computed FMOs of BTPS-4F and BTPS-4Cl. Calculated at B3LYP/6-31G (d,p) level.

Table 1. Optical parameters of BTPS-4F and BTPS-4Cl

Material	$\lambda_{onset,\ sol}$ (nm)[a]	$\lambda_{max,\ sol}$ (nm)[a]	ε_{max} ($M^{-1}\ cm^{-1}$)[a]	$\lambda_{onset,\ film}$ (nm)[b]	E_g (eV)[b,c]	$\Delta\lambda_{onset}$ (nm)
BTPS-4F	786	727	1.15×10^5	896	1.38	110
BTPS-4Cl	801	736	1.37×10^5	913	1.36	112

[a] In dilute chloroform solutions (1×10^{-5} M).
[b] In film states.
[c] Calculated from the absorption onset of the films.
[d] $\Delta\lambda_{onset} = \lambda_{onset,\ film} - \lambda_{onset,\ sol}$

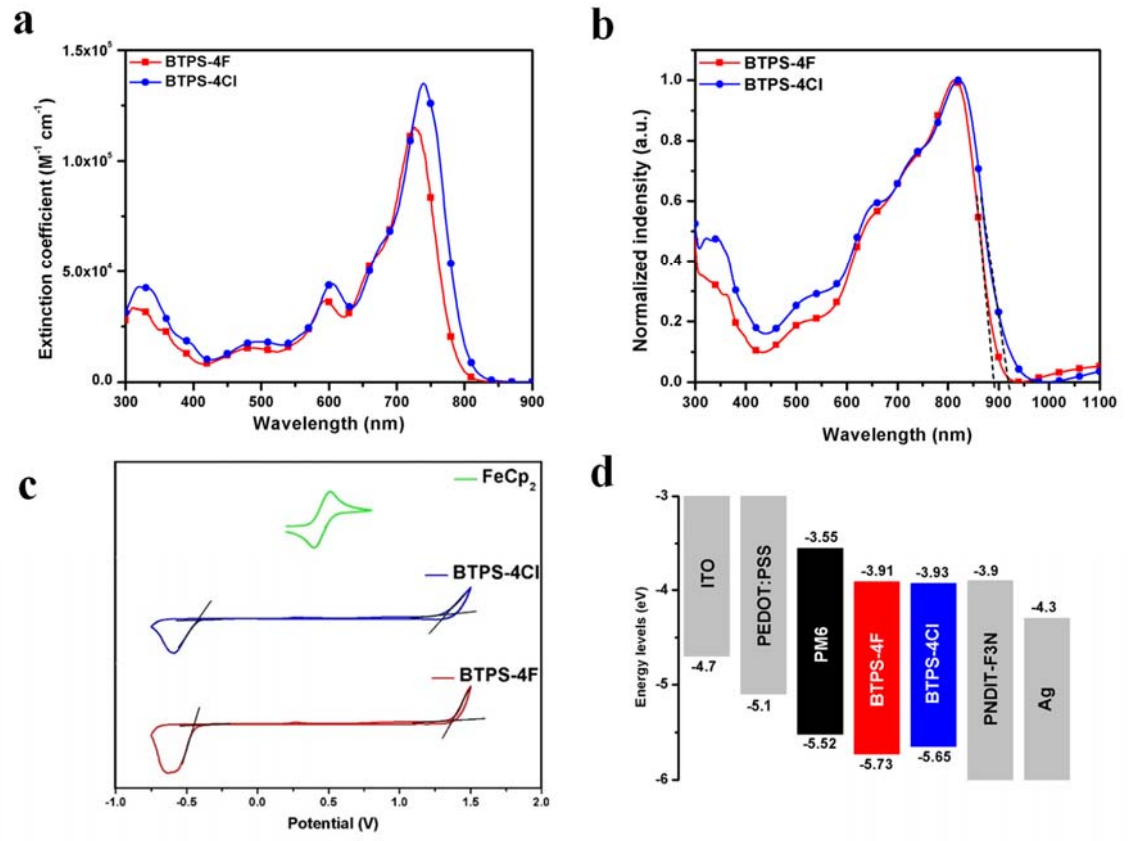

Figure 3. UV-vis spectra of BTPS-4F and BTPS-4Cl (a) in chloroform solutions and (b) in film states. (c) Cyclic voltammograms of $FeCp_2^{0/+}$, BTPS-4F and BTPS-4Cl. (d) Architecture and energy levels of BHJ devices. The conversion of reduction/oxidation onsets and LUMO/HOMO energy levels can be described as: $E_{LUMO} = -[e(E^{red} - E^{Fc/Fc+}) + 4.8]$; $E_{HOMO} = -[e(E^{ox} - E^{Fc/Fc+}) + 4.8]$

To investigate the optical properties of BTPS-4F and BTPS-4Cl, UV-visible (UV-Vis) absorption spectroscopy was employed to study the SMAs in dilute chloroform solutions and film states

(**Figure 3a-b, Table 1**). The absorption of BTPS-4F peaked at 727 nm, with a maximum extinction coefficient (ε_{max}) of 1.15×10^5 M^{-1} cm^{-1}, whereas that of BTPS-4Cl peaked at 736 nm, with an ε_{max} of 1.37×10^5 M^{-1} cm^{-1}. Thus, BTPS-4Cl exhibits a stronger and redshifted absorption compared to BTPS-4F, which is consistent with the higher polarizability of chlorine atoms and the smaller calculated bandgap of BTPS-4Cl. In film states, both BTPS-4F and BTPS-4Cl exhibit bathochromic absorptions relative to their absorptions in chloroform solutions with absorption onsets at 896 and 913 nm respectively, corresponding to bandgaps of 1.38 and 1.36 eV, which agree with their calculated band gaps and absorption onsets in solutions. As a result, the absorptions of both blends satisfactorily cover the solar spectrum from 300 to 900 nm.

Cyclic voltammetry (CV) (**Figure 3c**) was employed to investigate the effect of different end groups on energy levels. The LUMO and highest occupied molecular orbital (HOMO) levels of the species in film state were estimated from the onset reduction and oxidation potentials using ferrocene/ferrocenium (-4.8 eV) ($FeCp_2/FeCp_2^+$) as an external standard and plotted in **Figure 3d**. The LUMO of BTPS-4F (-3.91 eV) is slightly higher than that of BTPS-4Cl (-3.93 eV). It matches well with the slightly higher V_{OC} of BTPS-4F based devices (**Table 2**). The LUMO levels of the SMAs are also very close to that of the electron transport layer, PNDIT-F3N, hence promoting efficient charge collection.[43,44]

Table 2. Photovoltaic parameters[a] of devices based on PM6:BTPS-4F and PM6:BTPS-4Cl

Material	V_{OC} (V)	J_{SC} (mA cm^{-2})	FF	PCE, PCE_{max} (%)	μ_h, μ_e (10^{-4} cm^2 V^{-1} s^{-1})
PM6:BTPS-4F	0.82 ± 0.005	24.8 ± 0.4	0.76 ± 0.01	15.4 ± 0.5, 16.2	1.2 ± 0.1, 2.1 ± 0.1
PM6:BTPS-4Cl	0.80 ± 0.002	24.0 ± 0.5	0.68 ± 0.01	13.1 ± 0.3, 13.5	1.1 ± 0.1, 1.9 ± 0.1

[a] Average values from 15 devices for each material combinations.

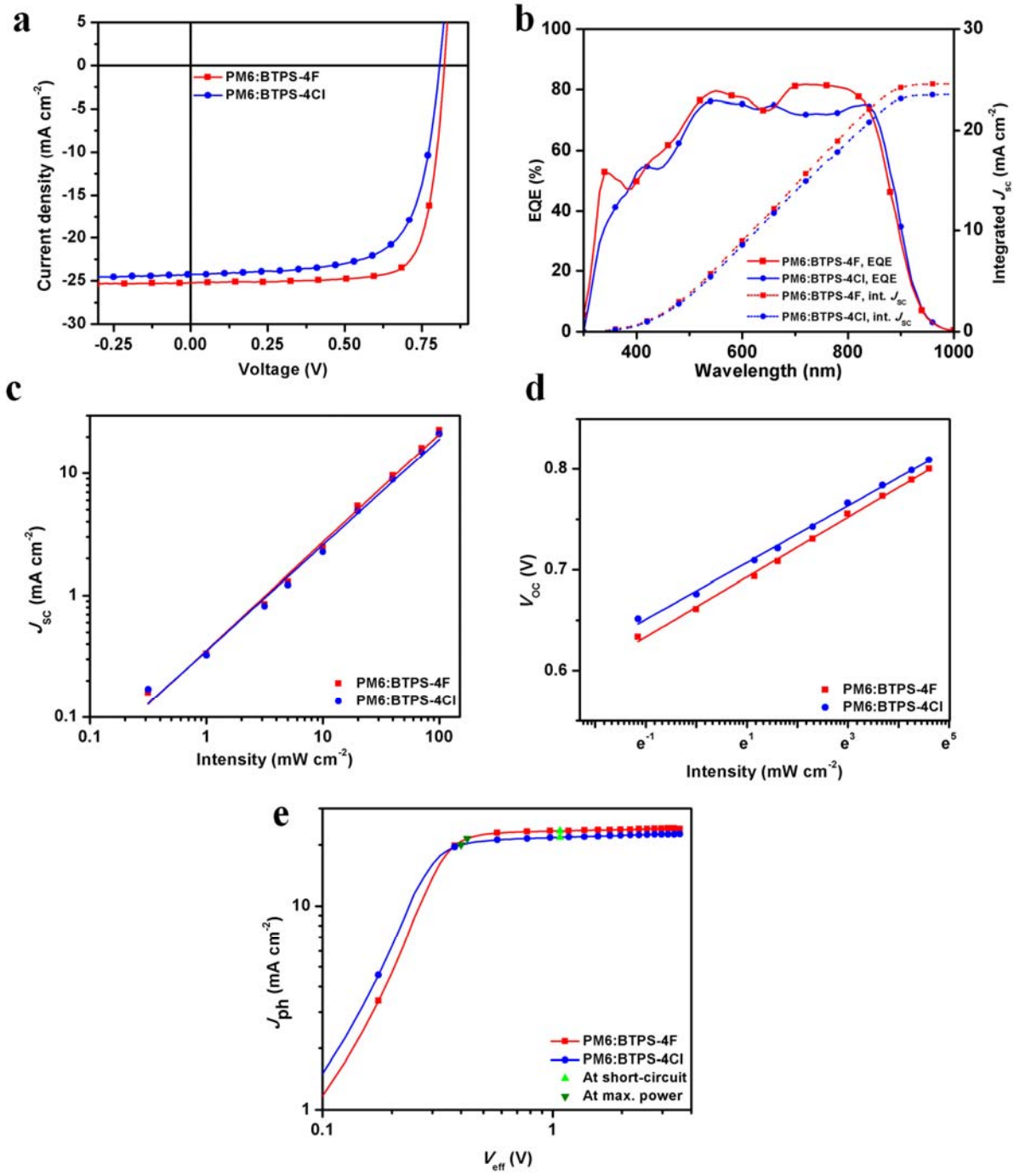

Figure 4. (a) *J-V* characteristics, (b) solid lines: external quantum efficiency (EQE) spectra and dashed lines: integrated J_{SC}, (c) light-intensity-dependence J_{SC} plots, (d) light-intensity-dependence V_{OC} plots and (e) photocurrent (J_{ph}) versus effective voltage (V_{eff}) plots of PM6:BTPS-4F and PM6:BTPS-4Cl devices.

The photovoltaic properties of PM6:BTPS-4F and PM6:BTPS-4Cl were then investigated with a conventional device structure of ITO/PEDOT:PSS/PM6:SMA/PNDIT-F3N/Ag and photovoltaic parameters of respective devices are summarized in **Table 2**. The higher shunt resistance R_{shunt} (73.49 kΩ cm^2 vs 68.89 kΩ cm^2) and lower series resistance R_{series} (0.50 Ω cm^2 vs 1.25 Ω cm^2) of BPTS-4F-based devices matched their better photovoltaic performance (**Figure S2** and **S3**).[45,46] Compared with Y6-based-devices when they were first reported, BTPS-4F-based ones achieved a better PCE and similar performance parameters. Considering the LUMO of BTPS-4F is higher than that of Y6, we believe there is still room for improvements on V_{OC} of BTPS-4F-based devices. Therefore, with further optimizations on molecular design and device fabrication, BTPS-4F and other alkylthio-containing NFAs have the potential to be another exemplary class of NFAs.

BTPS-4F-based devices achieved a slightly higher V_{OC} than that of BTPS-4Cl-based ones, which is consistent with the CV results. Due to the nearly identical bandgaps of the two SMAs, the higher V_{OC} of BTPS-4F-based devices indicates a smaller V_{loss} ($V_{loss} = E_g/q - V_{OC}$) than that of BTPS-4Cl-based devices (0.53 V vs 0.55 V).[47] Both materials exhibit satisfactory quenching efficiencies (BTPS-4F: 87.8% (785 nm excitation), 86.5% (514 nm excitation); BTPS-4Cl: 90.3% (785 nm excitation), 77.8% (514 nm excitation)) in photoluminescence (PL) experiments (**Figure S4, Table S1**), implying efficient exciton dissociation in both blends. The integrated J_{SC} values from EQE measurements are 24.56 mA cm^{-2} and 23.51 mA cm^{-2} respectively, which match the values found in *J-V* characteristics (**Figure 4a**). EQE plots (**Figure 4b**) reveal that both devices harvest photons efficiently in a broad absorption range. Furthermore, the higher J_{SC} of BTPS-4F-based devices is mainly due to the enhanced harvesting response of light from about 700 to 850 nm. It is interesting to note that the UV-vis absorption of PM6:BTPS-4F is lower in the range of 700 to 850 nm but the blend yields a better EQE in the same region than PM6:BTPS-4Cl does. The better SMA packing in BTPS-4F blend films is proposed to be the reason for the higher EQE despite its weaker absorption intensity. A discussion on film morphologies will be covered in later sections to support this point.

Charge recombination was studied with light-intensity-dependent experiments. *J-V* characteristics of the devices under varying light intensity are provided in **Figure S5**. Both devices were found to follow the typical relationship, $J_{SC} \propto P^{\alpha}$ (where P is the light intensity and α is a recombination index, **Figure 4c**). The α values are 0.89 and 0.87 for BTPS-4F- and BTPS-4Cl-based devices

respectively. The slopes of V_{OC} versus P (**Figure 4d**) are 1.15 and 1.10 k_BT/q for BTPS-4F-based and BTPS-4Cl-based devices, where k_B is Boltzmann constant, T is room temperature (298 K) and q is the elementary charge. The light-intensity dependent experiments indicate that recombination in both materials is sufficiently suppressed, resulting in satisfactory FFs for both BTPS-4F-based and BTPS-4Cl-based devices. Charge dissociation behaviors of respective devices were further studied by plotting photocurrent density (J_{ph}) against effective voltage (V_{eff}) (**Figure 4e**). J_{ph} equates the difference between current density under illumination (J_L) and under dark (J_D). V_{eff} is defined to be $V - V_0$, where V_0 is the voltage at which $J_{ph} = 0$. Dissociation probability (P(E,T)) can then be estimated by dividing J_{SC} values at short circuit and at maximum power by saturation photocurrent density (J_{sat}). BTPS-4F-based devices were found to exhibit higher dissociation probabilities at short circuit (J_{SC} / J_{sat}) (97.5% vs 96.5%) and at maximum power (J_{MP} / J_{sat}) (89.2% vs 88.8%) than BTPS-4Cl-based ones, indicating that BTPS-4F-based devices collect charges from excitons more effectively, hence resulting in a higher J_{SC}. Further studies on the photogeneration profile and recombination dynamics of PM6:BTPS-4F and PM6:BTPS-4Cl may be needed to provide more insights on the absorption and recombination behaviors at different wavelengths to explain the difference in EQE of respective materials more thoroughly.

The space-charge-limited-carrier method was employed to study the carrier mobilities of PM6:BTPS-4F and PM6:BTPS-4Cl blends (**Figure S6**). In the drift regime, $J^{1/2}$ directly varies with applied voltage (Mott-Gurney law) and hence respective carrier mobilities can be extracted. μ_h and μ_e of PM6:BTPS-4F blends are both higher than that of PM6:BTPS-4Cl blends. (**Table 2**). Besides, the mobility ratio (μ_h/μ_e) of PM6:BTPS-4F (0.57) is closer to unity than that of PM6:BTPS-4Cl (0.54). The enhanced charge carrier mobilities and a more balanced mobility ratio of PM6:BTPS-4F are beneficial to charge transport, resulting in an improved J_{SC} and a higher FF in BTPS-4F-based devices. Moreover, the more balanced mobilities in BTPS-4F-based devices may have contributed to the slightly larger α value.[48,49]

Various characterization techniques were then employed to study the molecular ordering and film morphology. Grazing incidence wide-angle X-ray scattering (GIWAXS) was performed on the pure and blend films to investigate the molecular packing of respective materials (**Figure 5**).[50] Both blends were found to adopt a dominant face-on molecular orientation with respect to the substrate, indicated by the strong (010) π–π stacking peaks in the 2-D patterns and the significant

(100) peaks of the out-of-plane linecuts. Therefore, π–π interactions between molecules can effectively contribute to the charge transport, leading to the satisfactory mobilities of both blends. The π-π spacings of BTPS-4F in pure films and blend films are 3.51 Å and 3.55 Å, respectively, both of which are smaller than those of BTPS-4Cl (3.53 Å and 3.58 Å for pure and blend films). Besides, the small π-π coherence lengths (CLs) of PM6:BTPS-4F (25.5 nm) and PM6:BTPS-4Cl (24.5 nm) are beneficial to charge transport. Consequently, the π-π stacking in PM6:BTPS-4F is noticeably more compact and ordered, in agreement with its superior carrier mobilities and J_{SC}.[51]

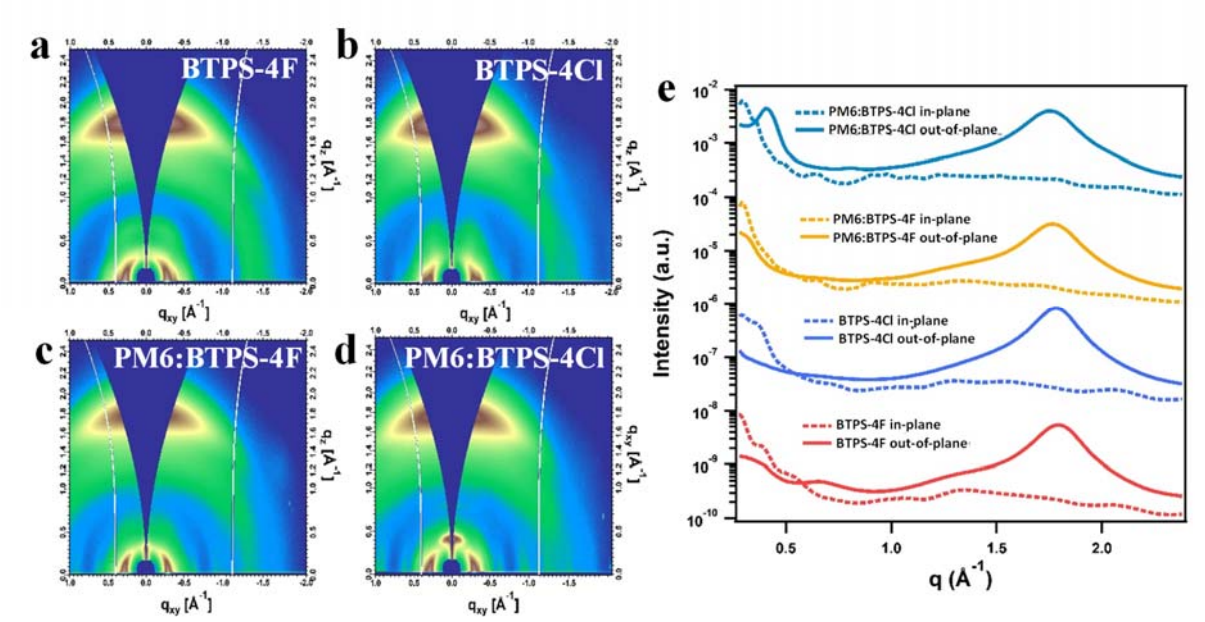

Figure 5. 2-D GIWAXS patterns of (a) BTPS-4F, (b) BTPS-4Cl, (c) PM6:BTPS-4F, (d) PM6:BTPS-4Cl. (e) 1-D GIWAXS profiles of out-of-plane (solid line) and in-plane (dashed line) directions.

Resonant soft X-ray scattering (R-SoXS) was employed to probe the nanoscale phase segregations of PM6:BTPS-4F and PM6:BTPS-4Cl films.[52–54] The Lorentz-corrected R-SoXS profiles of PM6:BTPS-4F and PM6:BTPS-4Cl films acquired at 283.8 eV are shown in **Figure 6**. The long periods of PM6:BTPS-4F and PM6:BTPS-4Cl are 62.8 nm and 89.8 nm respectively. A long period longer than the optimal diffusion length impairs exciton dissociation, since excitons may recombine before reaching the donor-acceptor interface or dispersed acceptor molecules.[55,56] Therefore, PM6:BTPS-4F exhibits higher exciton dissociation probabilities than PM6:BTPS-4Cl does, as also supported by the J_{ph} - V_{eff} plots (**Figure 4d**). Moreover, the relative composition variations, monotonically related to the domain purity of the polymer-rich domains, were

estimated to be 1.00 and 0.88 for PM6:BTPS-4F and PM6:BTPS-4Cl respectively.[57,58] It indicates that phase mixing is more uniform in PM6:BTPS-4F, which is consistent with the trends observed in R_{RMS} and long periods. Since a higher domain purity is crucial in suppressing recombination, the R-SoXS results agree well with the superior EQE response and FF of BTPS-4F-based devices.[59,60] In addition, atomic force microscopy (AFM) (**Figure S7**) reveals that the surface roughness of both blends were small, indicating proper mixing between PM6 and the NFAs. Thus, the morphology measurements may explain why BTPS-4F-based devices achieve superior overall performance.

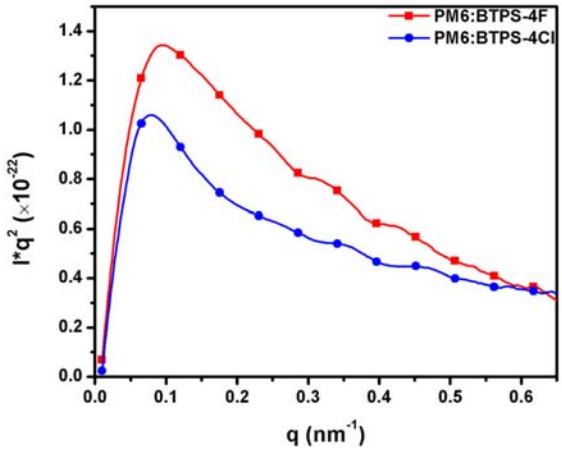

Figure 6. Lorentz-corrected R-SoXS profiles at 283.8 eV.

CONCLUSIONS

In this study, BTPS-4F and BTPS-4Cl, which are the first NFAs designed via attaching alkylthio chains to a Y6 structure, were investigated. The incorporation of undecylthio chains is shown to be a feasible strategy in fine-tuning NFAs. Despite showing a slightly weaker absorption from 700 to 850 nm, the enhanced packing of PM6:BTPS-4F enabled its devices to perform better than BTPS-4Cl-based devices do, as supported by GIWAXS and R-SoXS studies. As a result, BTPS-4F-based devices achieved a high performance, with a PCE up to 16.2%, whereas devices based on BTPS-4Cl achieved a PCE of 13.5%. This study demonstrates for the first time the effect of alkylthio side chains on fine-tuning Y6-like acceptor molecules by manipulating the energy levels and morphology, which would provide important guidelines to further studies on exciton dynamics and development of high-performance non-fullerene OSCs.

CONFLICTS OF INTEREST

There are no conflicts to declare.

ACKNOWLEDGEMENTS

The work described in this paper was partially supported by the Shen Zhen Technology and Innovation Commission (project number JCYJ20170413173814007, JCYJ20170818113905024), the Hong Kong Research Grants Council (Research Impact Fund R6021-18, project numbers 16305915, 16322416, 606012, and 16303917), Hong Kong Innovation and Technology Commission for the support through projects ITC-CNERC14SC01 and ITS/471/18), National Natural Science Foundation of China (NSFC, No. 91433202) and the National Key Research and Development Program of China (No. 2019YFA0705900) funded by MOST. X-ray data acquisition and manuscript input by NCSU authors are supported by ONR grant N000141712204 and N000142012155. X-ray data were acquired at beamline 7.3.3 of the Advanced Light Source, Lawrence Berkeley National Laboratory, which was supported by the Director, Office of Science, Office of Basic Energy Sciences, of the U.S. Department of Energy under Contract DE-AC02-05CH11231.

REFERENCES

1 Z. Li, J. Shan, L. Yan, H. Gu, Y. Lin, H. Tan and C.-Q. Ma, *ACS Appl. Mater. Interfaces*, 2020, DOI:10.1021/acsami.9b23366.

2 H. Ye, S. V. Kesava, J. F. M. Hardigree, R. E. Brown, G. Mazzotta, R. Warren, P. J. Skabara and M. Riede, *J. Mater. Chem. C*, 2020, **8**, 4909-4918.

3 Y. Lin, Y. Li and X. Zhan, *Chem. Soc. Rev.*, 2012, **41**, 4245–4272.

4 H. Li, J. Wang, Y. Wang, F. Bu, W. Shen, J. Liu, L. Huang, W. Wang, L. A. Belfiore and J. Tang, *Sol. Energy Mater. Sol. Cells*, 2019, **190**, 83–97.

5 M. Chang, Y. Wang, N. Qiu, Y. Q. Q. Yi, X. Wan, C. Li and Y. Chen, *Chinese J. Chem.*, 2017, **35**, 1687–1692.

6 G. Z. Yuan, H. Fan, S. S. Wan, Z. Jiang, Y. Q. Liu, K. K. Liu, H. R. Bai, X. Zhu and J. L. Wang, *J. Mater. Chem. A*, 2019, **7**, 20274–20284.

7 H. L. Yip and A. K. Y. Jen, *Energy Environ. Sci.*, 2012, **5**, 5994–6011.

8 L. Meng, Y. Zhang, X. Wan, C. Li, X. Zhang, Y. Wang, X. Ke, Z. Xiao, L. Ding, R. Xia, H. L. Yip, Y. Cao and Y. Chen, *Science (80-.).*, 2018, **361**, 1094–1098.

9 L. Zhan, S. Li, T. K. Lau, Y. Cui, X. Lu, M. Shi, C. Z. Li, H. Li, J. Hou and H. Chen, *Energy Environ. Sci.*, 2020, **13**, 635–645.

10 Y. Cui, H. Yao, L. Hong, T. Zhang, Y. Tang, B. Lin, K. Xian, B. Gao, C. An, P. Bi, W. Ma and J. Hou, *Natl. Sci. Rev.*, 2020, **7**, 1239-1246.

11 Y. Wang, B. Jia, J. Wang, P. Xue, Y. Xiao, T. Li, J. Wang, H. Lu, Z. Tang, X. Lu, F. Huang and X. Zhan, *Adv. Mater.*, 2020, **32**, 1–8.

12 J. Yuan, Y. Zhang, L. Zhou, C. Zhang, T. K. Lau, G. Zhang, X. Lu, H. L. Yip, S. K. So, S. Beaupré, M. Mainville, P. A. Johnson, M. Leclerc, H. Chen, H. Peng, Y. Li and Y. Zou, *Adv. Mater.*, 2019, **31**, 1–8.

13 R. Sun, T. Wang, Z. Luo, Z. Hu, F. Huang, C. Yang and J. Min, *Sol. RRL*, 2020, DOI: 10.1002/solr.202000156.

14 Q. Liu, Y. Jiang, K. Jin, J. Qin, J. Xu, W. Li, J. Xiong, J. Liu, Z. Xiao, K. Sun, S. Yang, X. Zhang and L. Ding, *Sci. Bull.*, 2020, **65**, 272–275.

15 Q. An, J. Wang, W. Gao, X. Ma, Z. Hu, J. Gao, C. Xu, M. Hao, X. Zhang, C. Yang and F. Zhang, *Sci. Bull.*, 2020, **65**, 538–545.

16 X. Ma, J. Wang, J. Gao, Z. Hu, C. Xu, X. Zhang and F. Zhang, *Adv. Energy Mater.*, 2020, **10**, 1–9.

17 M. J. Sung, M. Huang, S. H. Moon, T. H. Lee, S. Y. Park, J. Y. Kim, S. K. Kwon, H. Choi and Y. H. Kim, *Sol. Energy*, 2017, **150**, 90–95.

18 W. Yan, Q. Zhang, Q. Qin, S. Ye, Y. Lin, Z. Liu, Z. Bian, Y. Chen and C. Huang, *Dye. Pigment.*, 2015, **121**, 99–108.

19 Q. Wei, W. Liu, M. Leclerc, J. Yuan, H. Chen and Y. Zou, *Sci. China Chem.*, 2020, **63**, 1352-1366.

20 J. Yuan, Y. Zhang, L. Zhou, G. Zhang, H. L. Yip, T. K. Lau, X. Lu, C. Zhu, H. Peng, P. A. Johnson, M. Leclerc, Y. Cao, J. Ulanski, Y. Li and Y. Zou, *Joule*, 2019, **3**, 1140–1151.

21 Z. Luo, R. Sun, C. Zhong, T. Liu, G. Zhang, Y. Zou, X. Jiao, J. Min and C. Yang, *Sci. China Chem.*, 2020, **63**, 361–369.

22 H. Yu, R. Ma, Y. Xiao, J. Zhang, T. Liu, Z. Luo, Y. Chen, F. Bai, X. Lu, H. Yan and H. Lin, 2020, **4**, 2428-2434.

23 W. Zhu, A. P. Spencer, S. Mukherjee, J. M. Alzola, V. K. Sangwan, S. H. Amsterdam, S. M. Swick, L. O. Jones, M. C. Heiber, A. A. Herzing, G. Li, C. L. Stern, D. M. Delongchamp, K. L. Kohlstedt, M. C. Hersam, G. C. Schatz, M. R. Wasielewski, L. X. Chen, A. Facchetti and T. J. Marks, 2020, **142**, 14532-14547.

24 C. Zhu, J. Yuan, F. Cai. L. Meng, H. Zhang, H. Chen, J. Li, B. Qiu, H. Peng, S. Chen, Y. Hu, C. Yang, F. Gao, Y. Zou and Y. Li, *Energy Environ. Sci.*, 2020, **13**, 2459-2466.

25 L. Zhan, S. Li, T. K. Lau, Y. Cui, X. Lu, M. Shi, C. Z. Li, H. Li, J. Hou and H. Chen, *Energy Environ. Sci.*, 2020, **13**, 635–645.

26 Y. Wang, C. Zhuang, Y. Fang, H. Do Kim, H. Yu, B. Wang and H. Ohkita, *Nanomaterials*, 2020, **10**, 241.

27 M. Cheng, X. Yang, F. Zhang, J. Zhao and L. Sun, *J. Phys. Chem. C*, 2013, **117**, 9076–9083.

28 C. P. Hsieh, H. P. Lu, C. L. Chiu, C. W. Lee, S. H. Chuang, C. L. Mai, W. N. Yen, S. J. Hsu, E. W. G. Diau and C. Y. Yeh, *J. Mater. Chem.*, 2010, **20**, 1127–1134.

29 K. Rundel, S. Maniam, K. Deshmukh, E. Gann, S. K. K. Prasad, J. M. Hodgkiss, S. J.

Langford and C. R. McNeill, *J. Mater. Chem. A*, 2017, **5**, 12266–12277.

30 A. Tang, B. Xiao, F. Chen, J. Zhang, Z. Wei and E. Zhou, *Adv. Energy Mater.*, 2018, **8**, 1–9.

31 H. Yu, Z. Qi, X. Li, Z. Wang, W. Zhou, H. Ade, H. Yan, K. Chen, *Sol. RRL*, 2020, 10.1002/solr.202000421.

32 R. L. Elsenbaumer, D. S. Marynick, S. Seong and R. L. Meline, *Mater. Res. Soc. Symp. Proc.*, 1994, **328**, 221–225.

33 R. S. Glass, L. Adamowicz and J. L. Broeker, *J. Am. Chem. Soc.*, 1991, **113**, 1065–1072.

34 W. B. Motherwell, R. B. Moreno, I. Pavlakos, J. R. T. Arendorf, T. Arif, G. J. Tizzard, S. J. Coles and A. E. Aliev, *Angew. Chemie*, 2018, **130**, 1207–1212.

35 B. R. Beno, K. S. Yeung, M. D. Bartberger, L. D. Pennington and N. A. Meanwell, *J. Med. Chem.*, 2015, **58**, 4383–4438.

36 E. Salatelli, M. Marinelli, M. Lanzi, A. Zanelli, S. Dell'Elce, A. Liscio, M. Gazzano and F. Di Maria, *J. Phys. Chem. C*, 2018, **122**, 4156–4164.

37 B. Qiu, Z. Chen, S. Qin, J. Yao, W. Huang, L. Meng, H. Zhu, Y. Yang, Z. G. Zhang and Y. Li, *Adv. Mater.*, 2020, **1908373**, 1–9.

38 T. H. Lee, S. Oh, S. Rasool, S. Hong, C. E. Song, D. Kim, S. K. Lee, W. S. Shin and E. Lim, *J. Mater. Chem. A*, 2020, **8**, 10318-10330.

39 J. Gao, J. Ge, R. Peng, C. Liu, L. Cao, D. Zhang, F. Billy, L. Hong, E. Zhou and Z. Ge, *J. Mater. Chem. A*, 2020, **8**, 7405–7411.

40 Y. Ezhumalai, F. S. Lin, M. S. Fan, K. Prabakaran, J. S. Ni, Y. C. Wu, G. H. Lee, M. C. Chen and K. C. Ho, *ACS Appl. Mater. Interfaces*, 2020, **12**, 15071–15079.

41 S. L. Chang, K. E. Hung, F. Y. Cao, K. H. Huang, C. S. Hsu, C. Y. Liao, C. H. Lee and Y. J. Cheng, *ACS Appl. Mater. Interfaces*, 2019, **11**, 33179–33187.

42 Y. Zhang, Y. Cho, L. Zhong, Y. Wang, B. Huang, Z. Yuan, C. Yang, Y. Chen and Y. Li, *Sol. RRL*, 2020, DOI: 10.1002/solr.202000071.

43 W. Xu, F. He, M. Zhang, P. Nie, S. Zhang, C. Zhao, R. Luo, J. Li, X. Zhang, S. Zhao, W. Di Li, F. Kang, C. W. Nan and G. Wei, *ACS Energy Lett.*, 2019, **4**, 2491–2499.

44 F. Bu, B. He, Y. Ding, X. Li, X. Sun, J. Duan, Y. Zhao, H. Chen and Q. Tang, *Sol. Energy Mater. Sol. Cells*, 2020, **205**, 110267.

45 H. Yu, Z. Qi, J. Zhang, Z. Wang, R. Sun, Y. Chang, H. Sun, W. Zhou, J. Min, H. Ade and H. Yan, *J. Mater. Chem. A*, 2020, DOI: 10.1039/D0TA06658C.

46 J. Vollbrecht, V. V. Brus, S. J. Ko, J. Lee, A. Karki, D. X. Cao, K. Cho, G. C. Bazan and T. Q. Nguyen, *Adv. Energy Mater.*, 2019, **9**, 1901438.

47 J. Yuan, T. Huang, P. Cheng, Y. Zou, H. Zhang, J. L. Yang, S. Y. Chang, Z. Zhang, W. Huang, R. Wang, D. Meng, F. Gao and Y. Yang, *Nat. Commun.*, 2019, **10**, 1–8.

48 J. Vollbrecht, J. Lee, S.-J. Ko, V. Brus, A. Karki, W. Le, M. Seifrid, M. Ford, K. Cho, G. Bazan and T.-Q. Nguyen, *J. Mater. Chem. C*, 2020, DOI:10.1039/D0TC02136A.

49 L. J. A. Koster, V. D. Mihailetchi, H. Xie and P. W. M. Blom, *Appl. Phys. Lett.*, 2005, **87**, 1–3.

50 A. Hexemer, W. Bras, J. Glossinger, E. Schaible, E. Gann, R. Kirian, A. MacDowell, M. Church, B. Rude and H. Padmore, *J. Phys. Conf. Ser.*, 2010, **247**, 012007.

51 P. Müller-Buschbaum, *Adv. Mater.*, 2014, **26**, 7692–7709.

52 E. Gann, A. T. Young, B. A. Collins, H. Yan, J. Nasiatka, H. A. Padmore, H. Ade, A. Hexemer and C. Wang, *Rev. Sci. Instrum.*, 2012, **83**, 045110.

53 B. A. Collins, Z. Li, J. R. Tumbleston, E. Gann, C. R. Mcneill and H. Ade, *Adv. Energy Mater.*, 2013, **3**, 65–74.

54 H. Yu, L. Arunagiri, L. Zhang, J. Huang, W. Ma, J. Zhang and H. Yan, *J. Mater. Chem. A*,

2020, **8**, 6501–6509.

55 H. Yan, B. A. Collins, E. Gann, C. Wang, H. Ade and C. R. McNeill, *ACS Nano*, 2012, **6**, 677–688.

56 X. Jiao, L. Ye and H. Ade, *Adv. Energy Mater.*, 2017, **7**, 1–22.

57 S. Mukherjee, C. M. Proctor, J. R. Tumbleston, G. C. Bazan, T. Q. Nguyen and H. Ade, *Adv. Mater.*, 2015, **27**, 1105–1111.

58 L. Ye, H. Hu, M. Ghasemi, T. Wang, B. A. Collins, J. H. Kim, K. Jiang, J. H. Carpenter, H. Li, Z. Li, T. McAfee, J. Zhao, X. Chen, J. L. Y. Lai, T. Ma, J. L. Bredas, H. Yan and H. Ade, *Nat. Mater.*, 2018, **17**, 253–260.

59 S. Mukherjee, X. Jiao and H. Ade, *Adv. Energy Mater.*, 2016, **6**, 1–8.

60 S. Mukherjee, C. M. Proctor, G. C. Bazan, T. Q. Nguyen and H. Ade, *Adv. Energy Mater.*, 2015, **5**, 1–11.

TOC

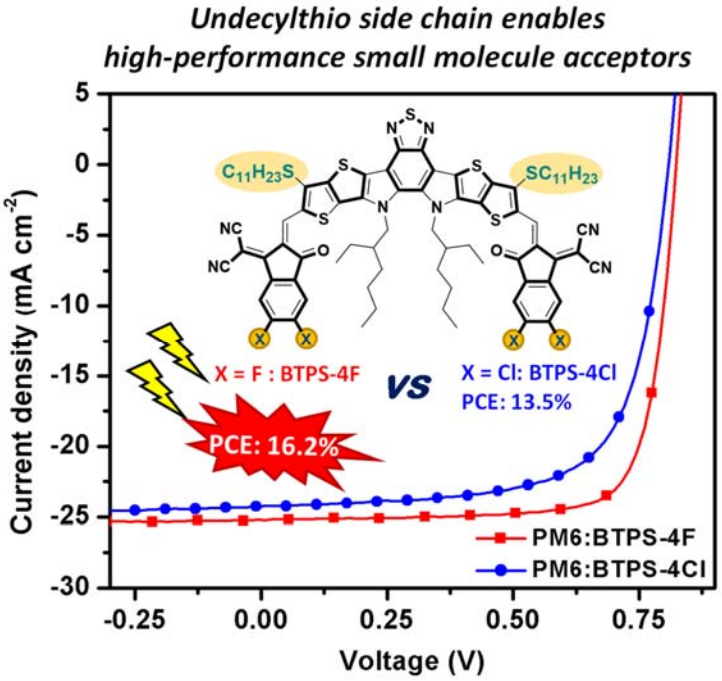
Undecylthio side chain enables
high-performance small molecule acceptors
Current density (mA cm-2)
Voltage (V)
X = F : BTPS-4F
PCE: 16.2%
vs
X = Cl: BTPS-4Cl
PCE: 13.5%
PM6:BTPS-4F
PM6:BTPS-4Cl